gels

Article

Optimization of Diclofenac Sodium-Loaded Alginate Microparticles: Chitosan-Assisted Encapsulation and pH-Dependent Release

Kamala Asgarova [1], İrem Toprakçı [1,*], Rabia Nur Bozkurt [1,2], Ebru Kurtulbaş [1], Barış Çağatay [1] and Selin Şahin [1]

[1] Department of Chemical Engineering, Faculty of Engineering, Istanbul University-Cerrahpaşa, 34320 Istanbul, Türkiye; kamala.asgarova@ogr.iuc.edu.tr (K.A.); rabia.bozkurt@istun.edu.tr (R.N.B.); ebru.kurtulbas@iuc.edu.tr (E.K.); baris.cagatay@iuc.edu.tr (B.Ç.); selins@iuc.edu.tr (S.Ş.)
[2] Department of Chemical Engineering, Faculty of Engineering and Natural Sciences, Istanbul Health and Technology University, 34445 Istanbul, Türkiye
* Correspondence: irem.toprakciyuksel@iuc.edu.tr

Abstract

Alginate microparticles offer a simple approach for drug encapsulation. However, their performance depends on formulation conditions. Diclofenac sodium (DCF) was encapsulated in alginate microparticles by ionic gelation. Sodium alginate concentration, $CaCl_2$ concentration and hardening time were optimized by Response Surface Method (RSM) using Box–Behnken design (RSM-BBD). Encapsulation efficiency (EE) varied considerably with the formulation conditions. The model showed a good fit ($R^2 = 0.9685$), while $CaCl_2$ concentration was the main factor affecting EE. The optimum conditions were 1.91% (w/v) sodium alginate, 4.99% (w/v) $CaCl_2$ and 23.4 min hardening time. The experimental EE was 80.34%, close to the predicted value of 80.41%. Chitosan was added to the optimized formulation at concentrations of 0.10–0.20% (w/v). EE increased with chitosan concentration and reached 93.85% at 0.20%. Drug release was studied in simulated gastric fluid (SGF) and simulated intestinal fluid (SIF). The release data were evaluated using zero-order, first-order, Higuchi and Korsmeyer–Peppas models. Characterization revealed a transition from a predominantly lamellar and fissured surface in the optimized alginate formulation to a more granular and highly textured architecture following chitosan incorporation, while the released fractions exhibited distinct hydrodynamic and electrokinetic characteristics. The addition of a low amount of chitosan therefore increased DCF encapsulation and changed its release behavior under gastrointestinal conditions.

Keywords: diclofenac sodium; alginate-chitosan; ionic gelation; microencapsulation; pH-dependent release; drug release kinetics

Check for updates

Academic Editors: Cheng Hu and Kongyin Zhao

Received: 25 September 2026
Revised: 26 October 2026
Accepted: 28 October 2026
Published: 1 November 2026

Copyright: © 2026 by the authors. Licensee MDPI, Basel, Switzerland. This article is an open access article distributed under the terms and conditions of the Creative Commons Attribution (CC BY) license.

1. Introduction

Alginate is a naturally derived anionic polysaccharide, which is a great value to pharmaceutical and biomedical due to its biocompatibility, biodegradability, regenerability, low toxicity and ease of gelation [1]. It can undergo ionotropic gelation in the presence of multivalent cations such as Ca^{2+}. Ca^{2+} is extensively used as crosslinking ions since it interacts with the carboxylate groups of alginate chains within guluronic acid-rich regions. So, this system produces the characteristic ionically crosslinked network commonly described by the "egg-box" model [2].

Ionic gelation enables the formation of alginate-based particulate carriers in which active compounds can be entrapped within a three-dimensional polymer network. Beyond facilitating drug encapsulation, the hydration and swelling behaviour of this network plays an important role in controlling drug release. Protonation of alginate carboxyl groups and the formation of alginic acid reduce matrix swelling in acidic environments, which might limit drug diffusion. As the pH increases, enhanced hydration and ion exchange promote swelling and relaxation of the polymer network. So, this facilitates drug diffusion and release [3]. However, these pH-responsive properties are highly dependent on the structure and integrity of the ionically crosslinked network, which are governed by the formulation and processing conditions. Therefore, while alginate-based particulate systems are particularly attractive for oral drug delivery, their performance must be carefully optimized to achieve reproducible drug encapsulation and controlled release. The polymer concentration determines solution viscosity and polymer-chain density, whereas the amount of Ca^{2+} available for ionic crosslinking affects the compactness and integrity of the gel network. Gelation or hardening time can influence the extent of ion diffusion and network development. Variations in these parameters might influence drug retention and encapsulation efficiency [4–8]. Since these factors might also interact with one another, one-factor-at-a-time (OFAT) optimization is insufficient to fully characterize the formulation space. Response surface methodology (RSM) with Box–Behnken experimental design (RSM-BBD) is an appropriate mathematical and statistical tool for quantifying individual and interaction effects, developing predictive models and identifying formulation conditions that maximize a desired response while reducing the number of experimental runs.

Another important point in this approach is that combining alginate with a second biopolymer represents one strategy for modifying the structure and functionality of the gel network [9]. Chitosan as a cationic polysaccharide containing protonatable amino groups can interact electrostatically with the negatively charged carboxylate groups of alginate. Formation of alginate-chitosan polyelectrolyte complexes can generate many advantages such as being an additional interfacial polymeric barrier, altering network compactness and permeability, and influencing encapsulation and drug transport [10]. These properties have resulted in extensive investigation of alginate-chitosan systems for oral and controlled drug delivery [11].

Diclofenac sodium (DCF) is a suitable model compound for investigating these effects. Its incorporation into alginate-based particulate matrices and its release are strongly influenced by polymer composition, crosslinking conditions and environmental pH [12,13]. Therefore, considering formulation-dependent encapsulation and gastrointestinal pH-dependent release simultaneously is important during developing alginate-based diclofenac carriers.

The present study aimed to develop DCF-loaded alginate microparticles by ionic gelation through optimizing the primary alginate-Ca^{2+} formulation via RSM-BBD. First, the effects of sodium alginate concentration, calcium chloride concentration and hardening time on encapsulation efficiency were evaluated. Then, numerical optimization and experimental validation was conducted. Later, the optimized alginate formulation was modified using low concentrations of chitosan to investigate its additional influence on drug encapsulation. Finally, the functional consequences of this modification were assessed through pH-dependent in vitro drug release, kinetic modeling of the release mechanism and physicochemical and morphological characterization.

2. Results and Discussion

2.1. Preliminary Formulation Studies

Preliminary experiments were conducted to establish suitable formulation conditions prior to RSM-BBD optimization. The amount of DCF was fixed at 0.01 g, while a hardening time of 20 min was used during the preliminary evaluation. Both alginate and alginate-chitosan systems were initially investigated to assess their suitability for microparticle formation. The formulation conditions and the corresponding EE values obtained during the preliminary studies are presented in Table 1.

Table 1. Preliminary formulation conditions and encapsulation performance of DCF-loaded alginate and alginate-chitosan microparticles.

Formulation	Sodium Alginate (%, w/v)	Calcium Chloride (%, w/v)	Chitosan (% w/v)	Hardening Time (min)	EE (%)	Observation *
1	1.5	3.5	-	20	51.830	
2	1.5	1.5	0.35	20	40.524	
3	1.5	2	0.35	20	44.242	
4	1.5	3.5	0.35	20	45.589	
5	1.5	5	0.35	20	38.334	
6	1.5	6	0.35	20	34.468	
7	1.5	3.5	0.7	20	-	Particle adhesion and heterogeneous surface.
8	1.5	3.5	1	20	-	Particle adhesion and heterogeneous surface.

* EE could not be determined for formulations containing 0.70 and 1.00% (w/v) chitosan because the increased viscosity and particle adhesion prevented the formation of homogeneous microparticles.

First, the effect of $CaCl_2$ concentration was examined over the range of 1.5–6.0% (w/v) as shown in Table 1. In formulations containing 0.35% (w/v) chitosan, changes in $CaCl_2$ concentration markedly affected the encapsulation performance. The EE values were 40.524, 44.242, 45.589, 38.334 and 34.468% at $CaCl_2$ concentrations of 1.5, 2.0, 3.5, 5.0 and 6.0% (w/v), respectively. Although increasing the $CaCl_2$ concentration initially improved DCF retention, an increase more than 3.5% resulted in a reduction in EE. This behavior suggests that the extent of ionic cross-linking must be carefully controlled, since excessive cross-linking might alter the structure of the polymeric network and adversely affect drug retention [14]. A similar concentration-dependent effect was reported by Celli et al., who observed a decrease in encapsulation efficiency when the $CaCl_2$ concentration was increased from 2 to 3% (w/v) in calcium-alginate microparticles [15].

The feasibility of incorporating chitosan was also evaluated during the preliminary experiments as seen in Table 1. Increasing the chitosan concentration to 0.7 and 1.0% (w/v) resulted in highly viscous formulations, accompanied by particle adhesion and heterogeneous surface characteristics. These findings indicate that chitosan concentration is an important formulation parameter affecting microparticle formation. Consistent with this observation, Takka and Gürel (2010) reported that chitosan concentration significantly influenced both particle size and encapsulation efficiency in alginate-chitosan beads [16]. Under these conditions, uniform microparticles could not be obtained. In contrast, the chitosan-free alginate formulation prepared using 1.5% (w/v) sodium alginate and 3.5% (w/v) $CaCl_2$ exhibited an EE of 51.830%, representing the highest value obtained among the preliminary formulations.

To conclude, the preliminary findings indicated that relatively high chitosan concentrations were unsuitable for obtaining uniform microparticles under the investigated preparation conditions. Therefore, chitosan was excluded from RSM-BBD optimization stage.

2.2. Encapsulation Efficiency and Drug Loading of DCF-Loaded Alginate Microparticles

The experimental conditions generated by the RSM-BBD and the corresponding EE values are presented in Table 2. Considerable variation in EE was observed across the 17 experimental runs, demonstrating the influence of the investigated formulation and process variables on DCF encapsulation. EE ranged from 14.82 to 80.08%. The highest EE (80.08%) was obtained in Run 4, corresponding to 2.0% sodium alginate, 5.0% $CaCl_2$ and a hardening time of 20 min. In contrast, the lowest EE (14.82%) was observed in Run 8, (2.0% sodium alginate combined with 2.0% $CaCl_2$ for 20 min). The remarkable difference between these two formulations shows that calcium concentration plays an important role in the encapsulation process as the cross-linker concentration. The statistical contribution of the individual formulation variables and their interactions is examined in detail in Sections 2.3 and 2.4.

Table 2. Experimental conditions of the RSM-BBD and corresponding encapsulation efficiency of DCF-loaded alginate microparticles.

No	A: Sodium Alginate (%, w/v)	B: Calcium Chloride (%, w/v)	C: Hardening Time (min)	EE * (%)
1	1.5	5	30	68.44
2	1.5	3.5	20	53.11
3	1.5	2	30	23.79
4	2	5	20	80.08
5	2	3.5	30	48.53
6	1	5	20	61.84
7	1.5	3.5	20	47.21
8	2	2	20	14.82
9	1	3.5	10	52.80
10	1.5	3.5	20	56.15
11	1	2	20	40.09
12	1.5	3.5	20	63.70
13	1.5	3.5	20	52.88
14	1.5	2	10	28.04
15	1	3.5	30	40.18
16	1.5	5	10	66.99
17	2	3.5	10	34.24

* Values represent the mean encapsulation efficiency obtained from three independently prepared formulations ($n = 3$) for each experimental condition. Each independent formulation was analyzed using three technical UV–Vis measurements.

In addition to EE, the amount of DCF incorporated per 50 mg of dried microparticles and the corresponding drug loading (DL) values were determined as complementary indicators of formulation performance. The amount of incorporated DCF varied from 0.159 to 0.632 mg per 50 mg of dried microparticles, corresponding to DL values ranging from 0.317 to 1.263% (Table 3). Run 4, with the highest EE, contained 0.425 mg DCF per 50 mg of dried microparticles and showed a DL of 0.849%. However, the highest DL (1.263%) was obtained in Run 11 in spite of its substantially lower EE of 40.09%. Run 8 exhibited both the lowest EE (14.82%) and the lowest DL (0.317%).

Table 3. Amount of DCF incorporated per 50 mg of dried microparticles and corresponding drug loading values obtained from RSM-BBD experimental runs.

No	DCF Amount (mg/50 mg Dried Microparticles)	DL (%)
1	0.422	0.844
2	0.402	0.803
3	0.253	0.506
4	0.425	0.849
5	0.334	0.668
6	0.542	1.084
7	0.382	0.763
8	0.159	0.317
9	0.543	1.086
10	0.411	0.821
11	0.632	1.263
12	0.393	0.786
13	0.326	0.652
14	0.289	0.578
15	0.346	0.691
16	0.366	0.732
17	0.259	0.518

These findings demonstrate that EE and DL did not vary proportionally across all experimental conditions. This distinction is expected because EE represents the fraction of the initially added drug successfully retained within the microparticles, whereas DL expresses the amount of incorporated drug relative to the final dry mass of the microparticles [17]. Consequently, changes in formulation composition and the resulting microparticle mass can influence DL independently of EE. Therefore, EE and DL should be considered complementary rather than interchangeable indicators of encapsulation performance. In the present study, EE was used as the response variable for RSM-BBD optimization, while DL was evaluated as a descriptive parameter. Indeed, review articles on alginate-based drug delivery systems specifically emphasize that encapsulation efficiency and drug loading capacity are distinct performance indicators, and that high encapsulation efficiency should not necessarily be expected to result in high drug loading capacity [18–20].

Kulkarni et al. reported that the encapsulation efficiency of diclofenac sodium-loaded alginate beads ranged from 30% to 71%, while the gel matrix density increased significantly with the degree of Ca^{2+}-mediated cross-linking [21]. However, it was specifically emphasized that although increased polymer matrix density facilitates drug retention within the gel structure, the amount of drug carried per unit mass of bead or microparticle remains limited to the milligram range. Similarly, while high encapsulation efficiencies (up to ≈98%) were achieved for diclofenac sodium in alginate-PVP K30 microspheres developed by Nayak et al. [22].

These findings demonstrate that maximizing the fraction of drug retained during microparticle formation does not necessarily maximize the drug content per unit mass of dried microparticles. Since the primary objective of the present optimization was to minimize drug loss during ionic gelation, EE was prioritized as the optimization criterion. Nevertheless, DL remains an important complementary parameter for evaluating the practical drug-carrying capacity of the formulations. Accordingly, the optimized formulation should be regarded as optimal with respect to EE within the investigated experimental design space, rather than as a formulation simultaneously optimized for both EE and DL.

2.3. Statistical Modelling and Analysis of Encapsulation Efficiency

The experimental EE data obtained from the 17 RSM-BBD runs were fitted to a quadratic model. The quadratic regression equation obtained in terms of coded factors is expressed by Equation (1).

$$Y = 54.61 - 2.15\,A + 21.332\,B - 0.1412\,C + 10.88\,AB + 6.73\,AC + 1.43\,BC - 4.14\,A^2 - 1.26\,B^2 - 6.53\,C^2 \quad (1)$$

where Y, A, B and C represent the coded values of encapsulation efficiency, sodium alginate concentration, $CaCl_2$ concentration and hardening time, respectively. The signs and magnitudes of the regression coefficients describe the direction and relative contribution of the corresponding terms within the fitted model. In particular, the comparatively large positive coefficient of B indicates a strong positive contribution of $CaCl_2$ concentration to EE within the investigated design space. However, the statistical relevance of each coefficient was determined from the ANOVA rather than from coefficient magnitude alone. The adequacy and statistical significance of the model were evaluated by ANOVA as given in Table S2. The resulting quadratic model was statistically significant ($F = 23.91$ and $p = 0.0002$), whereas the lack of fit was not significant ($F = 0.0480$ and $p = 0.9842$). This shows that the model adequately represented the experimental data within the investigated design space.

On the other hand, the model exhibited a high coefficient of determination ($R^2 = 0.9685$). this means that 96.85% of the variability in EE was accounted for by the fitted model. The adjusted R^2 (0.9280) and predicted R^2 (0.9350) were also in close agreement, which is below the commonly accepted threshold of 0.20 for agreement between these statistics [23]. A coefficient of variation (CV) below 10% is generally considered indicative of acceptable experimental precision in response surface modelling [24]. So, our finding is satisfying.

2.4. Effects of Formulation Variables on Encapsulation Efficiency

Analysis of the individual model terms showed that $CaCl_2$ concentration was the most statistically significant main factor affecting EE ($F = 169.55$, $p < 0.0001$). In contrast, the individual linear effects of sodium alginate concentration and hardening time were not statistically significant at $p > 0.05$. Significant interaction effects were observed for sodium alginate concentration × $CaCl_2$ concentration ($p < 0.05$) and sodium alginate concentration × hardening time ($p < 0.05$). The quadratic term for hardening time (C^2) was also significant ($p < 0.05$), suggesting a nonlinear relationship between hardening time and EE. Conversely, the BC, A^2 and B^2 terms were not statistically significant ($p > 0.05$).

The relative importance of these model terms was also evident from the standardized-effect plots (Figure 1). B, AB, AC and C^2 exceeded the critical reference value of 2.36 at $\alpha = 0.05$ as seen in the Pareto chart (Figure 1a). This finding is consistent with their statistical significance in the ANOVA (Table S2). The linear effect of $CaCl_2$ concentration exhibited the largest standardized effect by a substantial margin. The AB interaction showed the second-largest significant effect, followed by AC and C^2 (Figure 1a). A, C, BC, A^2 and B^2 remained below the significance threshold.

The normal probability plot of the standardized effects (Figure 1b) additionally illustrates the direction of the significant effects. $CaCl_2$ concentration (B) and the AB and AC interaction terms exhibited positive standardized effects, whereas C^2 showed a negative standardized effect. The positive effect associated with B is consistent with an overall increase in predicted EE with increasing $CaCl_2$ concentration within the studied range. In contrast, the negative quadratic coefficient of C^2 (−6.53) together with its statistical significance demonstrates curvature in the response to hardening time rather than a simple linear effect. These interaction and nonlinear effects are examined further using the response surface and contour plots in Section 2.5.

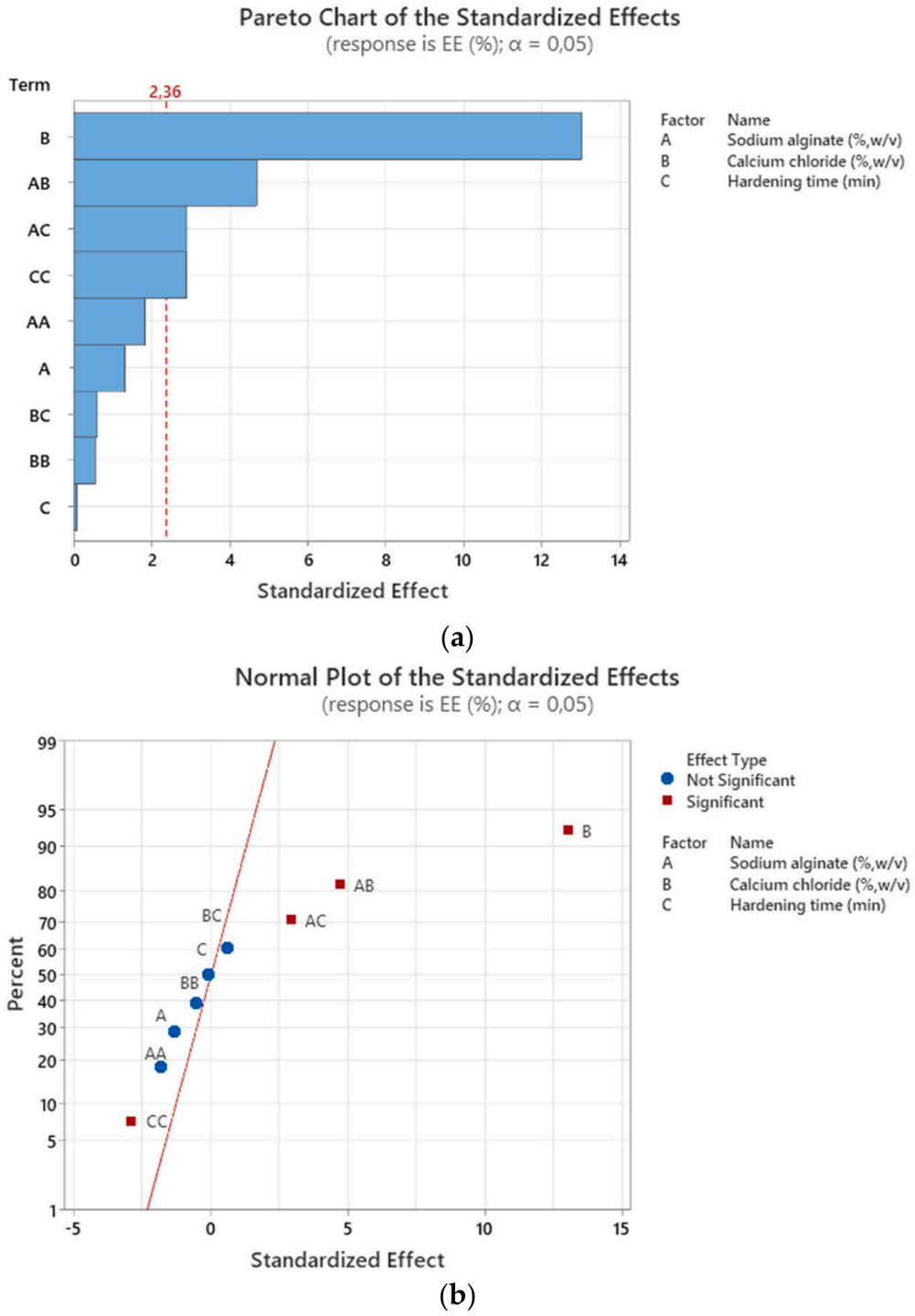
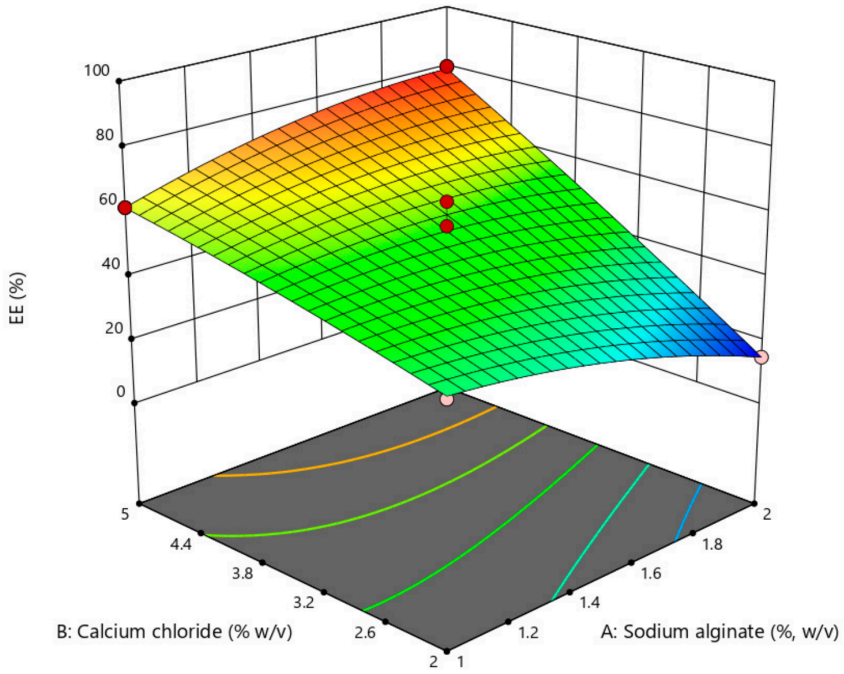


Figure 1. Standardized effects of formulation and process variables on the encapsulation efficiency of DCF-loaded alginate microparticles in the RSM-BBD: (**a**) Pareto chart of standardized effects and (**b**) normal probability plot of standardized effects. The reference line in the Pareto chart indicates the significance threshold at α = 0.05.

2.5. Response Surface and Contour Plot Analysis of Encapsulation Efficiency

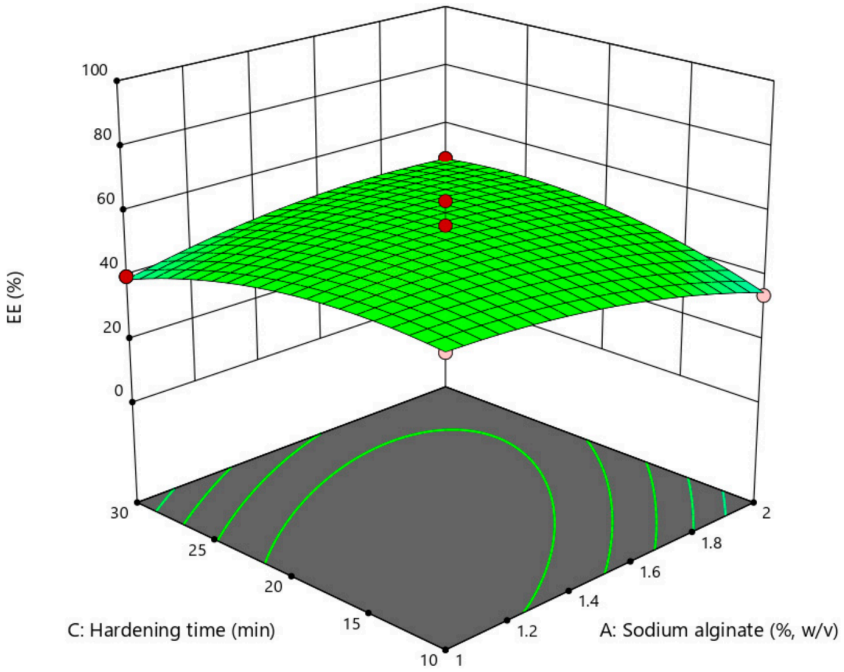
The combined effects of the variables were also examined using three-dimensional response surface (Figure 2) and two-dimensional contour plots (Figure 3). Figure 2a illustrates the combined effect of sodium alginate and $CaCl_2$ concentrations on EE at a fixed hardening time (20 min). This trend is also clearly reflected in the corresponding contour plot (Figure 3a), where the highest predicted EE region (>70%) was located at the upper

end of the investigated $CaCl_2$ range. However, the influence of sodium alginate concentration varied according to the $CaCl_2$ level as indicated by the curvature of the contour boundaries (Figure 3a). This tendency is consistent with the statistical results (Table S2), where $CaCl_2$ concentration was identified as the dominant main factor ($p < 0.0001$), while the AB interaction was also significant ($p < 0.05$). The pronounced influence of $CaCl_2$ concentration observed in the present study is consistent with previous findings for diclofenac sodium-loaded alginate microparticles. Nayak et al. reported an increase in drug entrapment efficiency from 78.23% to 85.77% as the $CaCl_2$ concentration was increased from 8.6% to 10.3% in plain alginate microbeads [22]. The authors also identified $CaCl_2$ concentration as a significant formulation variable affecting drug entrapment efficiency. This concentration-dependent behavior might be associated with Ca^{2+}-mediated ionic interactions with the carboxylate groups of alginate, which promote formation of the cross-linked alginate network. The characteristics of calcium-alginate gels are known to depend on both polymer-related properties and the concentration of divalent cross-linking ions [25]. More recently, response surface optimization of antibiotic-loaded calcium alginate systems similarly identified $CaCl_2$ concentration as a major factor governing encapsulation efficiency [4]. This trend is also consistent with studies reporting that polymer and cross-linker concentrations are determining factors for encapsulation efficiency in various drug-loaded calcium alginate and chitosan-based systems [21,22,26]. Ramdhan et al. demonstrated that increasing $CaCl_2$ concentration enhances the interaction of Ca^{2+} ions with the guluronic acid regions of alginate, causing an increase in gel strength. So, this enhanced Ca^{2+}-mediated cross-linking might contribute to the higher EE observed at increasing $CaCl_2$ concentrations in the present study by promoting the formation of a more strongly cross-linked alginate network [27].

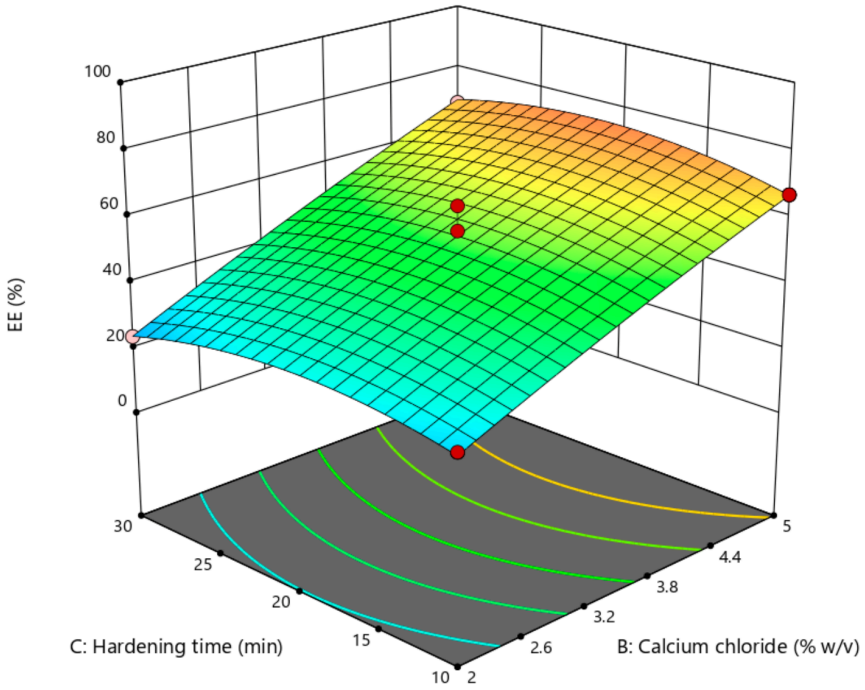


(**a**)

Figure 2. *Cont.*



(**b**)



(**c**)

Figure 2. Three-dimensional response surface plots showing the effects of (**a**) sodium alginate and $CaCl_2$ concentrations at a fixed hardening time of 20 min, (**b**) sodium alginate concentration and hardening time at a fixed $CaCl_2$ concentration of 3.5% (w/v), and (**c**) $CaCl_2$ concentration and hardening time at a fixed sodium alginate concentration of 1.5% (w/v) on the predicted encapsulation efficiency of DCF-loaded alginate microparticles.

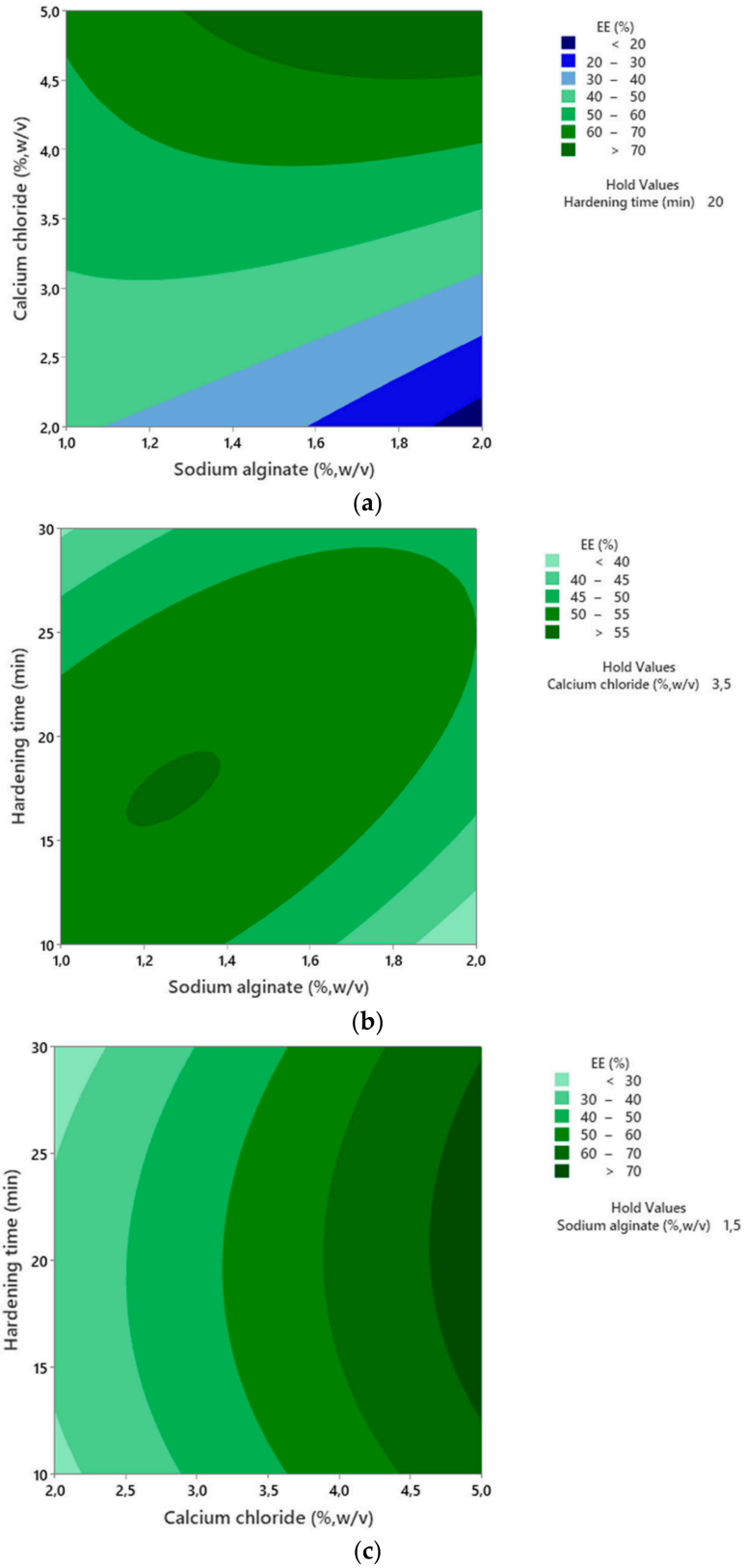


Figure 3. Two-dimensional contour plots showing the effects of (**a**) sodium alginate and $CaCl_2$ concentrations at a fixed hardening time of 20 min, (**b**) sodium alginate concentration and hardening time at a fixed $CaCl_2$ concentration of 3.5% (w/v), and (**c**) $CaCl_2$ concentration and hardening time at a fixed sodium alginate concentration of 1.5% (w/v) on the predicted encapsulation efficiency of DCF-loaded alginate microparticles.

The effects of sodium alginate concentration and hardening time produced a curved response surface (Figure 2b). The corresponding contour plot (Figure 3b) also shows a nonuniform response across the experimental region. This behavior agrees with the nonsignificant linear effects of sodium alginate concentration ($p > 0.05$) and hardening time ($p > 0.05$), in addition to the significant AC interaction ($p < 0.05$) and C^2 term ($p < 0.05$). So, hardening time did not independently produce a simple linear change in EE. Its effect depended on sodium alginate concentration and exhibited curvature within the investigated range. A comparable nonlinear behavior has been reported for alginate-based microcapsules, where encapsulation efficiency varied nonlinearly with increasing alginate concentration [28]. A similar interdependence between alginate concentration and time has been reported by Dodero et al. [29], who found a significant interaction between these variables in determining the effective crosslinking degree of ionically gelled alginate hydrogels. Alkhatib et al. described the curing of alginate beads as a diffusion-dependent process in which Ca^{2+} progressively penetrates the alginate matrix, while higher alginate concentrations can enhance cross-linking and improve the retention of encapsulated material [30]. This supports the observation that alginate concentration should be considered together with the cross-linking conditions rather than as an isolated formulation variable.

A different response pattern was observed for the combined effects of $CaCl_2$ concentration and hardening time at a fixed sodium alginate concentration of 1.5% (Figure 2c). The response surface increased sharply with $CaCl_2$. The contour plot (Figure 3c) supports this observation, with the EE regions distributed predominantly according to $CaCl_2$ concentration. This pattern is consistent with the strong statistical contribution of B and the nonsignificant BC interaction ($p > 0.05$). Generally, the color distributions observed in the contour plots (Figure 3) demonstrate that EE reaches maximum values within specific factor ranges and does not exhibit a linear increase. These visual findings are consistent with the identification of calcium chloride as the most dominant factor (Figure 1a). The higher-response regions in the contour plots indicate combinations of factor levels associated with increased predicted EE within the investigated design space. These model-derived response patterns were subsequently used for numerical optimization.

2.6. Optimization and Validation of DCF-Loaded Alginate Microparticles

Design-Expert software generated 100 possible solutions for DCF-loaded alginate beads based on the multi-objective optimization through RSM-BBD. The solution with the highest desirability value was selected as the optimum condition (Figure 4), since a desirability value approaching 1 represents a better fit to the optimization criteria [31].

At the optimum conditions, the sodium alginate concentration was determined to be approximately 1.91% (w/v), the calcium chloride concentration 4.99% (w/v), and the hardening time approximately 23.4 min (Table S3). Verification tests were performed under the conditions suggested by the Design-Expert software. Table S3 presents a comparison of the optimum parameters determined by RSM-BBD with the predicted and experimental EE values obtained under these conditions. The experimentally obtained EE value (80.34%) showed a high level of agreement with the EE value predicted by the model (80.41%). This agreement indicates that the developed model is statistically reliable.

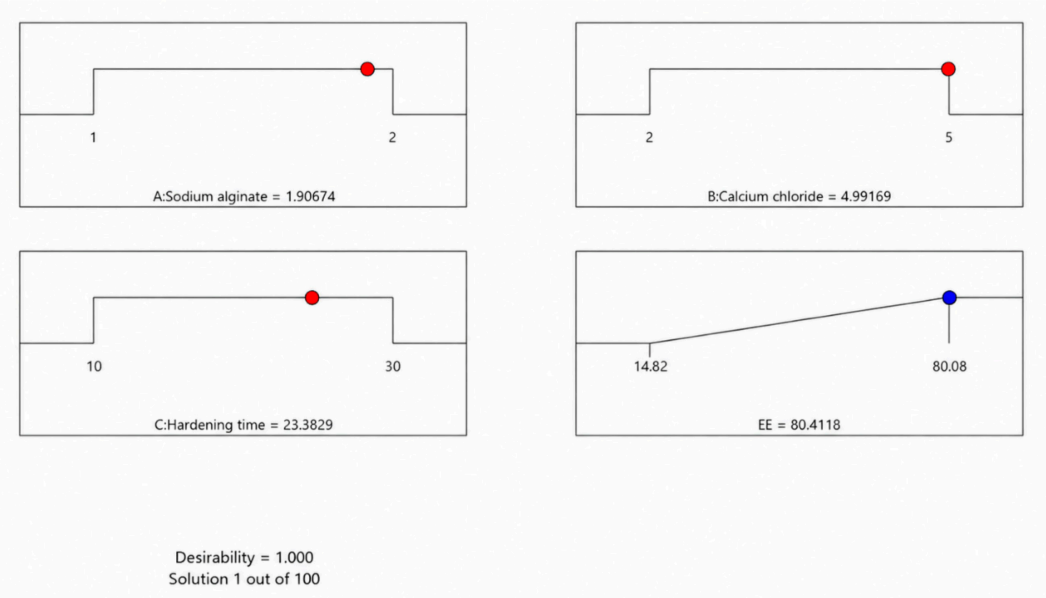


Figure 4. Numerical optimization and desirability plot showing the optimized levels of sodium alginate concentration, $CaCl_2$ concentration and hardening time for maximizing the predicted encapsulation efficiency of DCF-loaded alginate microparticles.

2.7. Effect of Chitosan Incorporation on Encapsulation Performance

Low concentrations of chitosan (0.10–0.20%, w/v) were evaluated to improve the encapsulation performance (Table 4), after optimization of the alginate formulation. Increasing the chitosan concentration from 0.10 to 0.20% increased EE from 80.79 to 93.85%. However, the observed differences should be interpreted cautiously in the absence of a verified statistical comparison between the formulations. This increase might be related to the electrostatic interaction between the positively charged amino groups of chitosan and the negatively charged carboxyl groups of alginate [32–34]. These interactions can form a more compact alginate-chitosan matrix and improve drug retention within the particles. These interactions can produce a more compact alginate–chitosan network and improve the retention of the encapsulated drug [35].

Table 4. Effect of low chitosan concentrations on encapsulation efficiency and drug loading under the optimized alginate formulation conditions *.

Chitosan (% w/v)	Encapsulation Efficiency (%)	Drug Loading (%)
0.10	80.79 ± 7.59 **	1.183 ± 0.111
0.15	87.25 ± 8.22	1.247 ± 0.117
0.20	93.85 ± 6.78	1.109 ± 0.080

* All experiments were performed using the optimized sodium alginate concentration, $CaCl_2$ concentration, and hardening time. ** Values are expressed as mean ± standard deviation from three independently prepared formulations ($n = 3$). Each formulation was analyzed using three technical UV–Vis measurements.

DL did not show the same trend. The DL value increased from 1.183% at 0.10% chitosan to 1.247% at 0.15%. However, DL decreased to 1.109% when the chitosan concentration was increased to 0.20%. Therefore, it did not provide the highest DL although the highest chitosan concentration resulted in the highest EE. The decrease in DL at 0.20% chitosan might be associated with the increased polymer content of the formulation and the resulting change in the drug-to-matrix ratio. A similar trend was reported by Hou et al., who observed that drug loading initially increased with increasing chitosan concentration but decreased

at higher chitosan concentrations [36]. Similarly, chitosan-based nanoparticles produced drug loading, which increased up to a certain polymer concentration, and then decreased at a higher concentration [37].

In addition to its role in modifying the encapsulation performance of alginate-based microparticles, chitosan and its derivatives have also attracted attention for their potential antibacterial properties. Piegat et al. investigated the antibacterial activity of an N,O-acylated chitosan derivative [38]. However, antibacterial activity may depend on the chemical structure of chitosan and the characteristics of the resulting formulation. Since antibacterial activity was not evaluated in the present study, no conclusions can be drawn regarding the antibacterial functionality of the developed alginate-chitosan microparticles. Further investigations could explore this property as an additional aspect of their biological characterization.

2.8. Physicochemical and Morphological Characterization of Microparticles

2.8.1. FTIR Analysis

FTIR analysis was performed on sodium alginate, calcium chloride ($CaCl_2$), diclofenac sodium (DCF), diclofenac sodium loaded alginate beads (OPT), chitosan (CS) and chitosan-containing diclofenac loaded alginate beads (0.2% CS-containing OPT) to analyze ionic gelation of SA in the presence of $CaCl_2$, encapsulation of DCF and incorporation of CS into OPT formulation. The corresponding FTIR spectra are presented in Figure 5. FTIR spectrum of sodium alginate exhibited its characteristic peaks at 1594, 1405, 1081 and 1021 cm^{-1}, correspond to asymmetric and symmetric stretching vibrations of carboxylate groups (COO^-), stretching vibrations of C-O bond of mannuroate and stretching vibrations of C-O and C-C bonds of guluronate respectively [39,40]. The absorption bands observed at wavenumbers of 3397 and 1631 cm^{-1} in the FTIR spectrum of $CaCl_2$ are associated with stretching and bending vibrations of crystal water [41]. In the FTIR spectrum of DCF, absorption bands at 1602, 1573 and 1497 cm^{-1} can be attributed to C=C bonds present in the phenyl ring. The peaks at 1555 and 1397 cm^{-1} are related to asymmetric and symmetric stretching vibrations of carboxylate groups (COO^-), respectively. The peak at 744 cm^{-1} is associated with vibrations of C-Cl bonds [42]. Absorption bands related with carboxylate groups of sodium alginate is widely used to interpreter the relationship between calcium ions and sodium alginate. When the FTIR spectrum of OPT were examined, the absorption bands at 1598 and 1425 cm^{-1} is attributed with asymmetric and symmetric stretching vibrations of carboxylate groups. Considering that the peaks of carboxylate groups are observed at 1594 and 1405 cm^{-1} in the sodium alginate, the shifts from 1594 to 1598 cm^{-1} and from 1405 to 1425 cm^{-1} suggest the ionic crosslinking of alginate with calcium ions [43]. In the FTIR spectrum of CS, the peaks at 3352 and 3284 cm^{-1} correspond to stretching vibrations of O-H and N-H groups, the absorption bands at 2919 and 2866 cm^{-1} is related with asymmetric and symmetric stretching vibration of C-H bonds, the peaks at 1647, 1565 and 1310 cm^{-1} can be identified as Amide I, Amide II and Amide III bands, respectively. Also, the peak at 1565 cm^{-1} can be attributed to amino groups on CS. Presence of absorbance bands belonging to the amide and amino groups confirms that CS is not completely deacetylated. The peaks at 1417 and 1372 cm^{-1} are associated with bending vibrations of methylene (CH_2) and methyl (CH_3) groups and lastly absorption bands at 1060 and 1023 cm^{-1} can be attributed to stretching vibrations of C-O-C and C-O bonds [44,45]. In the region 1650–1400 cm^{-1}, 0.2% CS-containing OPT are showed several peaks at 1639, 1546 and 1460 cm^{-1}. The new peak appeared at 1546 cm^{-1} is related to the deformation vibration of NH_3^+ group in the CS and presence of this peak suggest the interaction between protonated amine (NH_3^+) groups in the CS and the carboxylate groups in the OPT microparticles [46].

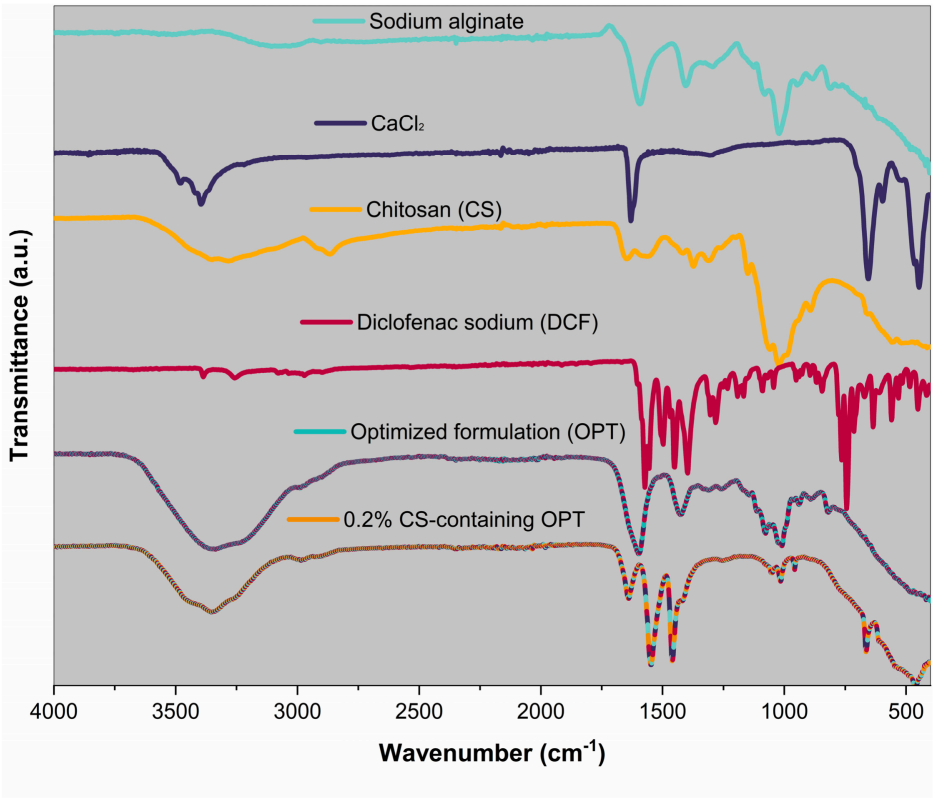


Figure 5. Comparative FTIR spectra of sodium alginate, $CaCl_2$, chitosan (CS), diclofenac sodium (DCF), the optimized formulation (OPT), and the 0.2% chitosan-containing optimized formulation (0.2% CS-containing OPT).

2.8.2. SEM Analysis

Scanning electron microscopy (SEM) was used to examine the surface morphology of the optimized DCF-loaded alginate microparticles (OPT) and the 0.2% (*w*/*v*) chitosan-containing formulation (0.2% CS-containing OPT) (Figure 6). The OPT microparticles exhibited a heterogeneous surface morphology, with relatively compact regions accompanied by irregular lamellar structures, grooves, and localized fissures (Figure 6a–d). At higher magnifications, pronounced folds and plate-like domains were evident across the surface of the dried calcium-alginate matrix. Similar surface irregularities have been reported for dried alginate-based microparticles and may be associated with structural rearrangement and shrinkage of the hydrated polymer network during drying [47,48].

Following chitosan incorporation, a pronounced alteration in surface morphology was observed (Figure 6e–h). In contrast to the predominantly lamellar appearance of OPT, the 0.2% CS-containing OPT exhibited a markedly rougher and more granular surface characterized by densely distributed microstructural domains. These features became particularly evident at higher magnifications (Figure 6g,h), where the surface displayed a highly textured architecture rather than the larger plate-like domains observed for OPT. This morphological alteration is consistent with previous observations in alginate–chitosan particulate systems, where chitosan coating has been reported to modify surface topography and produce a more irregular and wrinkled surface compared with uncoated alginate particles [49,50]. Overall, SEM analysis revealed a clear alteration in surface architecture following chitosan incorporation, characterized by a transition from a predominantly lamellar and fissured morphology to a more granular and highly textured surface. Nevertheless, these morphological observations alone do not provide direct evidence of changes in crosslinking density, network permeability, or swelling behavior.

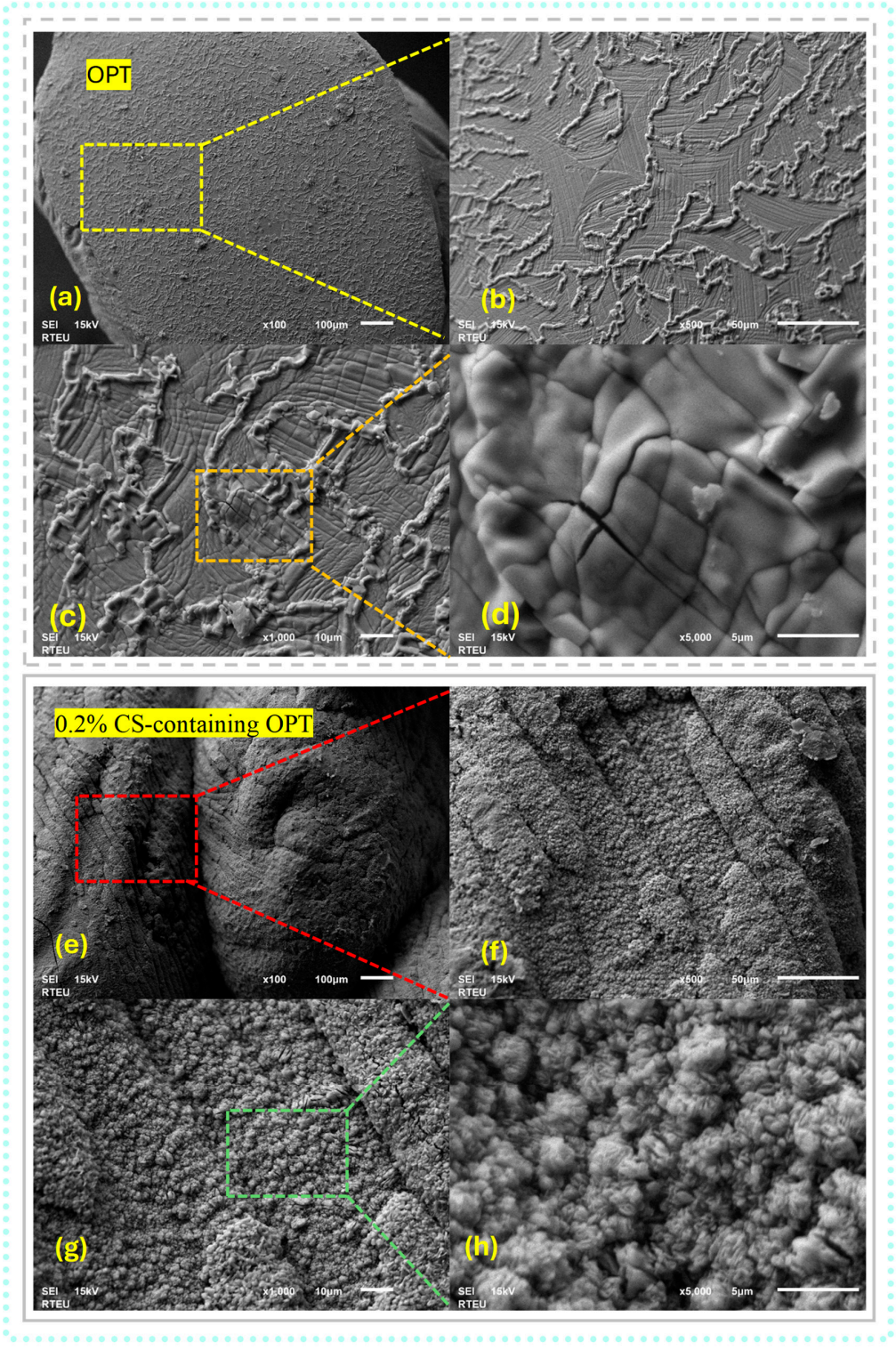


Figure 6. SEM micrographs of the optimized DCF-loaded alginate microparticles (OPT) (**a**–**d**) and 0.2% (*w*/*v*) chitosan-containing optimized microparticles (0.2% CS-containing OPT) (**e**–**h**) at increasing magnifications.

2.8.3. DLS and Zeta Potential Analysis

To characterize the species released into the surrounding medium, the release fractions obtained from OPT and 0.2% CS-containing OPT following incubation in phosphate-buffered saline (PBS, pH 6.8) were analyzed by DLS and electrophoretic light scattering (Figure 7). Accordingly, the resulting hydrodynamic size and zeta potential data represent

the dispersed populations present in the release medium rather than the dimensions or surface charge of the intact microparticles.

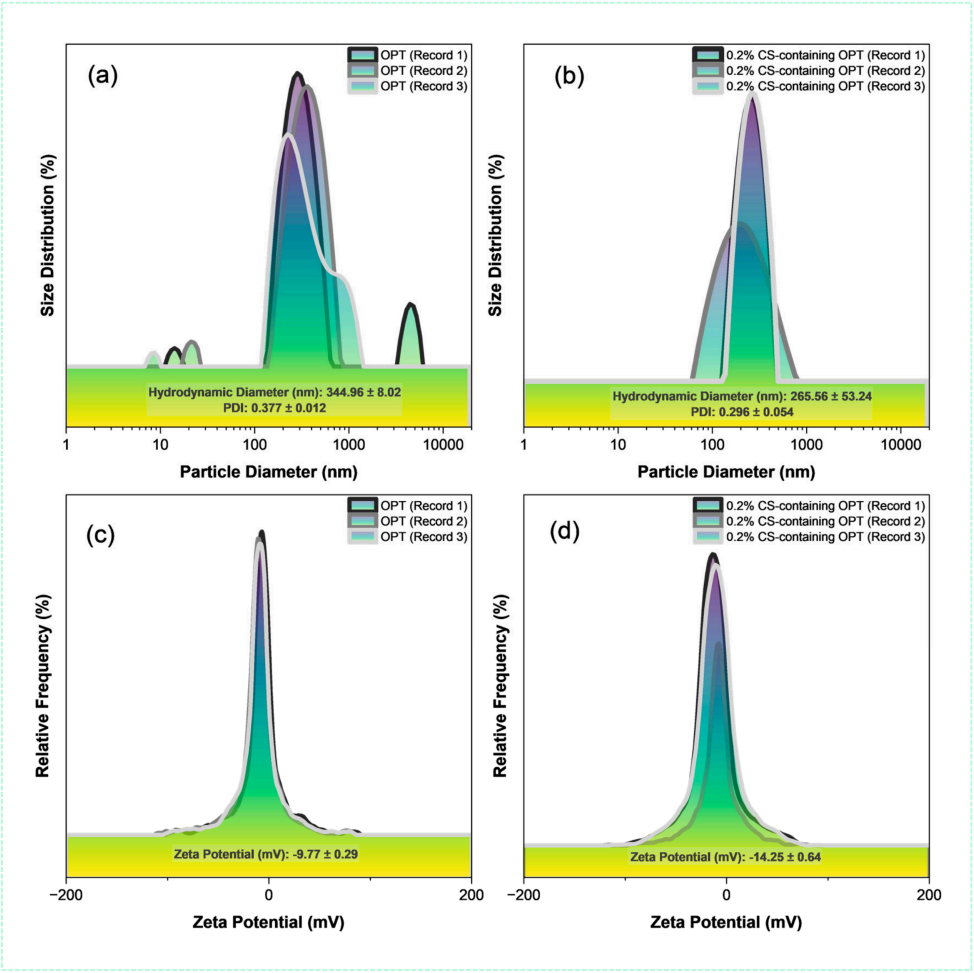


Figure 7. Hydrodynamic diameter distributions (**a**,**b**) and zeta potential distributions (**c**,**d**) of the release fractions obtained from OPT (**a**,**c**) and 0.2% (*w*/*v*) CS-containing OPT (**b**,**d**) after incubation in phosphate-buffered saline (PBS, pH 6.8). Values are expressed as mean ± SD of three consecutive measurements (Records 1–3) of the same sample.

The OPT-derived fraction exhibited an average hydrodynamic diameter of 344.96 ± 8.02 nm and a PDI of 0.377 ± 0.012 (Figure 7a). The size distribution was dominated by species within the 200–400 nm range, while minor signals were also observed below 25 nm and in the micrometer-size range, indicating a heterogeneous size distribution of the dispersed species. In comparison, the fraction obtained from 0.2% CS-containing OPT exhibited a smaller average hydrodynamic diameter of 265.56 ± 53.24 nm and a lower PDI of 0.296 ± 0.054 (Figure 7b), with the distribution predominantly centered around a single major population. Overall, these differences indicate that the populations dispersed from the uncoated and chitosan-containing matrices exhibited distinct hydrodynamic characteristics under the release conditions.

Both released fractions displayed unimodal zeta potential distributions, with mean values of −9.77 ± 0.29 mV for OPT and −14.25 ± 0.64 mV for 0.2% CS-containing OPT (Figure 7c,d), indicating an overall anionic interfacial character under the measurement conditions. Although chitosan is a cationic polysaccharide, its ionization is strongly pH-dependent, with an apparent pK_a of approximately 6.5; consequently, the protonation of its amino groups decreases as the environmental pH approaches and exceeds this value [51].

At pH 6.8, reduced protonation of chitosan may therefore contribute to the persistence of negative electrokinetic potentials, although it should not be regarded as the sole determinant of the measured values. Indeed, negative zeta potentials have been reported for alginate–chitosan systems, and the alginate-to-chitosan ratio has been shown to exert a pronounced influence on their electrokinetic characteristics [51,52]. In particular, increasing the relative proportion of alginate has been reported to shift the zeta potential of alginate–chitosan polyelectrolyte complexes toward more negative values [52].

The dispersed populations detected following release may be associated with structural relaxation and partial disintegration of the ionically cross-linked alginate matrix during incubation in the release medium [53]. Nevertheless, DLS determines the hydrodynamic size of dispersed species from their diffusion behavior and has recognized limitations in resolving heterogeneous and polydisperse systems [54]. Therefore, the more negative zeta potential measured for the 0.2% CS-containing OPT fraction should not be interpreted as evidence that chitosan rendered the surface of the original microparticles more negatively charged. Rather, when considered together with the differences in hydrodynamic diameter and PDI, the results demonstrate that the species dispersed from the uncoated and chitosan-containing matrices differed in their physicochemical characteristics under the release conditions. However, the precise chemical composition and structural identity of these dispersed species cannot be conclusively established from DLS and zeta potential measurements alone.

2.9. Release Kinetics and Mechanism of DCF from Alginate Microparticles

Table 5 presents the kinetic modeling results for diclofenac sodium release from pure alginate and 0.2% (w/v) chitosan-containing alginate microparticles in SGF and SIF. In the case of pure alginate microparticles in SGF, the Higuchi model showed the highest coefficient of determination ($R^2 = 0.9662$) compared with the zero-order ($R^2 = 0.9284$) and first-order ($R^2 = 0.9336$) models. This finding indicates that the experimental release profile was well described by the Higuchi model, suggesting that diffusion-related processes may contribute to DCF release under acidic conditions. However, the higher R^2 value alone does not establish diffusion as the predominant or sole release mechanism. The Korsmeyer–Peppas model yielded an n value of 0.6873, which may be consistent with anomalous (non-Fickian) transport under the assumptions commonly applied to spherical systems. This observation suggests the possible involvement of both drug diffusion and polymer relaxation or swelling, although these contributions cannot be conclusively distinguished from kinetic fitting alone [55]. This behavior is consistent with previous studies reporting pH-dependent release and diffusion-related mechanisms from alginate/chitosan-based DCF delivery systems [56].

In SIF, alginate microparticles showed a rapid initial release with more than 60% of the drug released at the first sampling point. The rapid initial release observed for pure alginate microparticles in SIF indicates that a substantial fraction of the encapsulated DCF was released at the earliest sampling point. Although the incorporation of 0.2% (w/v) chitosan was associated with changes in the overall release profile, the available quantitative results do not allow a reliable determination of the magnitude of any reduction in initial burst release. Therefore, the effect of chitosan on the initial release should be interpreted cautiously, and no definitive conclusion regarding burst-release suppression is drawn from the present data. The first-order ($R^2 = 0.8658$) and Higuchi ($R^2 = 0.8114$) models showed higher coefficients of determination than the zero-order model ($R^2 = 0.6724$), indicating comparatively poorer agreement with a constant-rate release model. Nevertheless, these differences in R^2 values do not independently establish a specific release mechanism. The rapid initial release may be associated with pH-dependent changes in the alginate matrix,

including possible swelling and ion-exchange processes, although these mechanisms were not directly quantified in the present study. Similar pH-dependent release profiles and rapid initial release have also been reported for chitosan-alginate microparticles [57].

Table 5. Kinetic model parameters for diclofenac sodium release from pure alginate and alginate containing 0.2% chitosan microparticles in simulated gastric fluid (SGF) and simulated intestinal fluid (SIF) *.

	GI System	Zero-Order Model		First-Order Model		Higuchi Model		Korsmeyer–Peppas Model **		
		k_0 (mg dk^{-1})	R^{2***}	k_1 (dk^{-1})	R^2	k_H (mg $dk^{-1/2}$)	R^2	n	K (dk^{-n})	R^2
Pure alginate microparticles produced under optimal conditions	SGF	0.0004	0.9284	0.0004	0.9336	0.0066	0.9662	0.6873	2.37×10^{-3}	0.8958
	SIF	0.0008	0.6724	0.0050	0.8658	0.0162	0.8114	-	-	-
Alginate containing 0.2% chitosan microparticles	SGF	0.0002	0.9647	0.0002	0.9263	0.0034	0.8953	0.6575	1.23×10^{-3}	0.9731
	SIF	0.0024	0.8200	0.0058	0.9080	0.0454	0.9268	0.2359	0.152	0.8158

* Time (t) was expressed in minutes (min). ** The Korsmeyer–Peppas model was applied only to the initial portion of the release profile, up to approximately 60% cumulative drug release. Korsmeyer–Peppas model was not applied for pure alginate microparticles in SIF, since cumulative drug release exceeded 60% at the first sampling point. *** The reported R^2 values describe the goodness of fit of the respective kinetic models and should not be interpreted as definitive evidence of a specific drug release mechanism. Korsmeyer–Peppas parameters refer only to the initial release region used for model fitting.

The addition of 0.2% (w/v) chitosan changed the release behavior. In SGF, the Korsmeyer–Peppas model provided the highest R^2 value (0.9731), followed by the zero-order model ($R^2 = 0.9647$). The release exponent ($n = 0.6575$) may be compatible with anomalous (non-Fickian) transport under the assumptions of the Korsmeyer–Peppas model for spherical particles. This finding suggests that diffusion and polymer relaxation or swelling could contribute to the release process, but it should not be regarded as definitive mechanistic evidence [58]. Regarding SIF, the Higuchi model showed the highest R^2 value (0.9268), followed by the first-order model ($R^2 = 0.9080$). The Korsmeyer–Peppas model gave a lower n value of 0.2359. However, the mechanistic interpretation of this exponent should be approached cautiously, since the model was applied only to the initial portion of the release profile.

The Higuchi release constant (k_H) for chitosan-containing microparticles increased from 0.0034 in SGF to 0.0454 in SIF, consistent with the faster drug release observed under SIF conditions. This pH-dependent behavior is consistent with studies on DCF-loaded pH-sensitive alginate/chitosan-based systems, which reported greater drug release under near-neutral conditions than under acidic gastric conditions [12].

To sum up, the kinetic models provide a comparative mathematical description of the experimental release profiles rather than definitive identification of the underlying release mechanisms. Although R^2 values are useful for evaluating goodness of fit, selecting the model with the highest R^2 does not by itself establish whether drug release is governed by diffusion, polymer relaxation, swelling, or a combination of processes. Furthermore, the Korsmeyer–Peppas model was fitted only to the initial portion of the release profiles, corresponding to approximately 60% cumulative drug release. Therefore, the calculated n values should be considered indicative of possible early-stage transport behavior and should not be extrapolated to the entire release process. Additional experimental evidence would be required to determine the relative contributions of the proposed mechanisms.

In the present study, drug release experiments were conducted separately in SGF and SIF to evaluate the release behavior of the formulations under two distinct pH conditions. Although this approach provides information on the pH-dependent release characteristics of the microparticles, it does not fully reproduce the sequential exposure to gastric and intestinal environments following oral administration. Therefore, the absence of a sequential SGF-to-SIF release experiment represents a limitation of the present study. Future investigations involving an initial incubation in SGF followed by transfer to SIF would provide a more representative assessment of the release performance of these formulations under simulated gastrointestinal transit conditions.

3. Conclusions

Diclofenac sodium-loaded alginate microparticles were prepared by ionic gelation. The formulation conditions were optimized using response surface approach. Cross-linker concentration was the main factor affecting EE. The experimental EE under the optimum conditions was 80.34%, which was close to the predicted value of 80.41%. Chitosan addition improved the encapsulation efficiency of DCF-loaded alginate microparticles. Encapsulation increased from 80.79% to 93.85% as the chitosan concentration increased from 0.10 to 0.20%. Morphological characterization showed that chitosan incorporation altered the surface architecture of the optimized alginate microparticles, resulting in a more granular and highly textured morphology. DLS and zeta potential analyses of the released fractions further revealed distinct hydrodynamic and electrokinetic characteristics between the uncoated and chitosan-containing formulations. Furthermore, chitosan incorporation was associated with changes in the DCF release profile under simulated gastrointestinal conditions. However, the available quantitative data does not establish the extent to which chitosan reduces the initial burst release in SIF. Therefore, further quantitative evaluation would be required to confirm a burst-release-suppressing effect. These results show that chitosan addition improved diclofenac sodium encapsulation and modified drug release of the alginate microparticles. Although the formulation was optimized for encapsulation efficiency, further multi-response optimization incorporating drug loading and release characteristics would be necessary to identify the most suitable formulation for oral drug delivery applications.

4. Materials and Methods

4.1. Materials

DCF was purchased from Tokyo Chemical Industry Co., Ltd. (Tokyo, Japan). Acetic acid, sodium alginate, chitosan and calcium chloride dihydrate ($CaCl_2 \cdot 2H_2O$) were supplied by Sigma-Aldrich (St. Louis, MO, USA). The chitosan used in this study was low-molecular-weight chitosan (catalog no. 448869) with a manufacturer-reported molecular weight range of 50,000–190,000 Da and a degree of deacetylation of 75–85%. Acetic acid was used for the preparation of chitosan solutions, while sodium alginate and chitosan served as the biopolymeric matrix. Calcium chloride was employed as the cross-linking agent. Distilled and ultrapure water (18 MΩ·cm) used throughout the experimental studies were produced using a Milli-Q water purification system (Millipore, Burlington, MA, USA).

4.2. Preparation of Diclofenac Sodium-Loaded Alginate Microparticles

DCF-loaded alginate microparticles were prepared by the ionic gelation method. Sodium alginate solutions were prepared at concentrations specified by RSM-BBD (1.0–2.0%, w/v). A fixed amount of DCF (0.01 g) was incorporated into each alginate solution, and the resulting drug-polymer mixtures were stirred until homogeneous.

The prepared formulations were introduced dropwise into aqueous calcium chloride solutions at a constant flow rate of 3.5 mL/min using a syringe pump (New Era Pump

Systems, Inc., Farmingdale, NY, USA) under gentle stirring at 275 rpm. The $CaCl_2$ concentration was varied between 2 and 5% (w/v), according to the experimental design. All $CaCl_2$ concentrations were expressed on a weight/volume basis using $CaCl_2 \cdot 2H_2O$. Upon contact with the $CaCl_2$ solution, ionic interactions between Ca^{2+} ions and the guluronic acid residues of alginate resulted in the formation of microparticles through the egg-box gelation mechanism. The formed microparticles were maintained in the cross-linking medium for 10–30 min (as an independent variable in RSM-BBD). Following gelation, the microparticles were separated from the cross-linking medium and dried under ambient conditions in a fume hood.

4.3. Preparation of Alginate-Chitosan Microparticles

Following optimization of the alginate-based formulation using the RSM-BBD approach, the effect of chitosan incorporation during ionic gelation was investigated under the optimized formulation conditions. Based on preliminary experiments, chitosan concentrations of 0.10, 0.15 and 0.20% (w/v) were selected for further evaluation.

Chitosan solutions were prepared at the selected concentrations in an aqueous solution containing 10 g/L glacial acetic acid. Following complete dissolution of chitosan, the pH of the solutions was adjusted using 10 N NaOH. Subsequently, 4.99 g of $CaCl_2 \cdot 2H_2O$ was directly dissolved in 100 mL of each chitosan solution, corresponding to a nominal concentration of 4.99% (w/v) based on the initial solution volume. The final pH of the cross-linking medium was adjusted to 4.5. The microparticles were prepared under the optimized conditions determined by RSM-BBD, corresponding to approximately 1.91% (w/v) sodium alginate and a hardening time of 23.4 min. Thus, chitosan was incorporated during microparticle formation rather than being applied as a separate coating to previously prepared alginate microparticles. The resulting alginate-chitosan microparticles were evaluated in terms of encapsulation efficiency to determine the effect of chitosan concentration on DCF encapsulation.

4.4. Determination of Encapsulation Efficiency and Drug Loading

The encapsulation efficiency (EE) of DCF was determined indirectly by measuring the amount of non-encapsulated drug remaining in the cross-linking medium after microparticle formation. The microparticles were separated from the medium after completion of the gelation process. The amount of free DCF in the collected supernatant was quantified by UV–Vis spectrophotometry (PG Instruments, T60/Leicestershire, England) at 276 nm. For quantitative determination, a calibration curve was constructed using DCF standard solutions at concentrations of 10, 20, 25, 40 and 50 ppm. A linear relationship between DCF concentration and absorbance was obtained over the investigated concentration range (10–50 ppm) as described by the regression equation $y = 0.0302x + 0.0359$, with a coefficient of determination of $R^2 = 0.9999$. The concentration of free DCF in the supernatant was calculated using this regression equation. The encapsulation efficiency was calculated according to Equation (2) [26]:

$$EE\ (\%) = \frac{W_1 - W_2}{W_1} \times 100 \quad (2)$$

where W_1 is the total amount of DCF initially added to the formulation (mg), whereas W_2 is the amount of non-encapsulated DCF detected in the supernatant (mg).

In addition to the indirect determination of encapsulation efficiency, the drug content of the dried microparticles was determined directly for the evaluation of drug loading (DL). For this purpose, approximately 0.07 g of dried microparticles was dispersed in 25 mL of phosphate buffer (pH 6.8) and subjected to ultrasonication in an ultrasonic bath (Weightlab Instruments, Istanbul, Türkiye) for 20 min until complete dissolution was achieved. The

DCF concentration in the resulting solution was determined by UV–Vis spectrophotometry at 276 nm using the corresponding calibration curve.

The amount of encapsulated DCF was calculated from the measured concentration and extrapolated to the total mass of dried microparticles obtained from each formulation. DL was expressed as the percentage ratio of the encapsulated DCF mass to the mass of dried microparticles, as shown in Equation (3). The DCF amount per 50 mg of dried microparticles presented in Table 3 was subsequently calculated from the corresponding DL values.

$$DL\ (\%) = \frac{W_{DCF}}{W_{MP}} \times 100 \quad (3)$$

where W_{DCF} is the mass of diclofenac sodium determined in the dried microparticles (mg), and W_{MP} is the corresponding mass of dried microparticles (mg).

4.5. In Vitro Release Profile of Diclofenac Sodium-Loaded Microparticles

The in vitro release behavior of DCF from the prepared microparticles was investigated under conditions simulating the gastrointestinal (GI) environment. Simulated gastric fluid (SGF, pH 1.2) and simulated intestinal fluid (SIF, pH 6.8) were used as the release media. 0.2 g of DCF-loaded microparticles was placed in 50 mL of the corresponding release medium and maintained under continuous agitation at 100 rpm. Samples were withdrawn from the release medium at predetermined time intervals and filtered prior to analysis. The concentration of released DCF was determined spectrophotometrically using the corresponding calibration data. After each sampling, the withdrawn volume was immediately replaced with an equal volume of fresh release medium to maintain a constant total volume throughout the experiment.

The cumulative amount of DCF released at each time was calculated by taking into account both the drug concentration in the release medium and the drug removed during previous sampling steps. The release profiles were expressed as cumulative drug release as a function of time.

Kinetic Modelling of Diclofenac Sodium Release

The release profiles of DCF from the microparticle formulations in SGF and SIF were analyzed using zero-order, first-order, Higuchi and Korsmeyer–Peppas kinetic models [59,60]. The zero-order model was used to assess approximately constant-rate drug release, whereas the first-order model was applied to evaluate release behavior dependent on the amount of drug remaining. The Higuchi model was selected to examine the agreement of the release data with a square-root-of-time relationship, while the Korsmeyer–Peppas model was used to characterize the initial-stage release behavior through an empirical power-law relationship. The coefficient of determination (R^2) was used to assess the goodness of fit of the models; however, a higher R^2 value was not considered sufficient to establish a definitive drug release mechanism.

The zero-order model was described by Equation (4):

$$Q_t = Q_0 + k_0 t \quad (4)$$

where Q_t (mg g^{-1}) is the amount of DCF released at time t, Q_0 (mg g^{-1}) is the initial amount of drug in the release medium. k_0 (mg min^{-1}) is the zero-order release rate constant.

The first-order model was expressed according to Equation (5).

$$\log C_t = \log C_0 - k_1 t \quad (5)$$

where C_0 (mg g^{-1}) is the initial amount of DCF associated with the microparticles. C_t (mg g^{-1}) is the amount of drug remaining in the microparticles at time t (min), while k_1 (min^{-1}) is the first-order release rate constant.

The Higuchi model was applied using Equation (6):

$$Q_t = k_H t^{1/2} \quad (6)$$

Korsmeyer–Peppas model was applied according to Equation (7) in order to investigate the mechanism governing DCF release. Korsmeyer–Peppas model was applied only to the initial portion of the release profile corresponding to approximately 60% cumulative drug release. Accordingly, the model was not applied when the cumulative release had already exceeded 60% at the first sampling point [61]. The calculated n values were used to assess the contribution of diffusion and polymer relaxation/swelling to the overall release mechanism [62].

$$\frac{M_t}{M_\infty} = kt^n \quad (7)$$

where M_t/M_∞ represents the fractional drug release at time t, K is the Korsmeyer–Peppas kinetic constant. Additionally, n is the release exponent characterizing the drug-release mechanism.

4.6. Physicochemical and Morphological Characterization of Microparticles

The optimized DCF-loaded alginate microparticles (OPT) and the corresponding 0.2% (w/v) chitosan-containing formulation (0.2% CS-containing OPT) were characterized by Fourier-transform infrared (FTIR) spectroscopy and scanning electron microscopy (SEM). FTIR spectra were recorded using a Bruker Tensor 27 spectrometer (Bruker, Ettlingen, Germany) over the wavenumber range of 4000–400 cm^{-1}. Surface morphology was examined using a JEOL JSM-6610 scanning electron microscope (JEOL, Tokyo, Japan). Prior to SEM imaging, the dried samples were coated with a thin layer of gold to ensure adequate electrical conductivity.

Dynamic light scattering (DLS) and zeta potential analyses were performed on the liquid fractions collected from the release studies of OPT and 0.2% CS-containing OPT using a Litesizer 500 instrument (Anton Paar, Graz, Austria). Prior to analysis, the samples were suitably diluted, and all measurements were conducted at 25 °C. The hydrodynamic diameter and polydispersity index (PDI) of the dispersed species present in the release medium were determined by DLS, while their electrokinetic characteristics were assessed by zeta potential measurements.

4.7. Box–Behnken Experimental Design and Statistical Analysis

A RSM based on a three-factor and three-level Box–Behnken design was employed to investigate and optimize the formulation parameters affecting the encapsulation of DCF in alginate microparticles. The experimental design and statistical analyses were performed using Design-Expert software (version 12.0.1.0, Stat-Ease Inc., Minneapolis, MN, USA).

Three formulation and process parameters (sodium alginate concentration, $CaCl_2$ concentration and hardening time) were selected as independent variables. Each factor was investigated at three coded levels (−1, 0 and +1) (Table S1). Sodium alginate concentration was varied from 1.0 to 2.0% (w/v), whereas $CaCl_2$ concentration changed from 2.0 to 5.0% (w/v). Hardening time was between 10 min and 30 min. Encapsulation efficiency was targeted for maximization, since the main objective of this study was to maximize the retention of the initially incorporated diclofenac sodium within the alginate microparticles during the ionic gelation process. EE directly reflects the proportion of the initially added drug successfully retained in the microparticles and therefore provides a relevant measure for evaluating the effects of formulation and processing conditions on drug encapsulation. In contrast, drug loading represents the amount of incorporated drug relative to the final dry mass of the microparticles and is consequently influenced by both drug retention and the

mass of the resulting polymeric matrix. Therefore, DL was evaluated as a complementary formulation performance parameter rather than an additional optimization response. This approach allowed the optimization to focus specifically on drug retention while separately assessing the drug content of the resulting microparticles. The RSM-BBD generated a total of 17 experimental runs with 5 replicates at the center point. Each experimental condition was independently prepared in triplicate ($n = 3$) to evaluate experimental reproducibility. For each independently prepared formulation, three technical measurements were performed using UV–Vis spectrophotometry. The technical measurements were averaged to obtain the EE of each independent formulation. The reported EE values represent the means of three independently prepared formulations rather than single measurements. The distinction between independent experimental replicates and technical measurements was maintained to avoid treating repeated instrumental measurements as independent experimental observations. Some parameters were maintained constant to minimize the influence of uncontrolled process variations. The amount of DCF was fixed at 0.01 g. The dispensing rate was kept constant at 3.5 mL/min, while the stirring speed of the cross-linking medium was 275 rpm.

The relationship between the selected independent variables and EE was evaluated by fitting the experimental data to an appropriate polynomial model. Analysis of variance (ANOVA) was performed to assess the statistical significance of the fitted model and individual model terms. Model adequacy was evaluated using the coefficient of determination (R^2), adjusted R^2, predicted R^2 and lack-of-fit test. Statistical significance was considered at $p < 0.05$. Additionally, Pareto charts and contour plots were generated using Minitab Statistical Software (version 22, Minitab LLC, State College, PA, USA).

Supplementary Materials: The following supporting information can be downloaded at: https://www.mdpi.com/article/10.3390/gels12110994/s1, Table S1: Independent variables and their coded levels and response variable used for the optimization of DCF-loaded alginate microparticles; Table S2: Analysis of variance for the quadratic model of encapsulation efficiency; Table S3: RSM-based numerical optimization of DCF-loaded alginate microparticles and comparison of the predicted and experimental encapsulation efficiency under the optimal conditions.

Author Contributions: Conceptualization, İ.T. and S.Ş.; methodology, İ.T., S.Ş., E.K. and K.A.; formal analysis, K.A., R.N.B. and B.Ç.; investigation, all authors; data curation, all authors; writing—original draft preparation, İ.T.; writing—review and editing, İ.T. and S.Ş.; supervision, İ.T. and S.Ş.; project administration, İ.T. All authors have read and agreed to the published version of the manuscript.

Funding: This research was funded by the Scientific Research Projects Coordination Unit of Istanbul University-Cerrahpaşa, under the General Research Project (GENAP), Project No. 38090.

Institutional Review Board Statement: Not applicable.

Informed Consent Statement: Not applicable.

Data Availability Statement: The data presented in this study are available from the corresponding author upon reasonable request.

Acknowledgments: During the preparation of this manuscript, the authors used OpenAI ChatGPT (GPT-5.5) for language refinement. The authors reviewed and edited the output and take full responsibility for the content of this publication.

Conflicts of Interest: The authors declare no conflicts of interest.

References

1. Puscaselu, R.G.; Lobiuc, A.; Dimian, M.; Covasa, M. Alginate: From Food Industry to Biomedical Applications and Management of Metabolic Disorders. *Polymers* **2020**, *12*, 1–30. [CrossRef]
2. Ručigaj, A.; Golobič, J.; Kopač, T. The Role of Multivalent Cations in Determining the Cross-Linking Affinity of Alginate Hydrogels: A Combined Experimental and Modeling Study. *Chem. Eng. J. Adv.* **2024**, *20*, 100678. [CrossRef]
3. Toprakçı, İ.; Kurtulbaş, E.; Bozkurt, R.N.; Şahin, S. Coordination-Driven Assembly of Alginate Networks: From Egg-Box Structures to Bioactive Delivery Applications. *Gels* **2026**, *12*, 774. [CrossRef]
4. Hebip, İ.; Toprakçı, İ.; Bozkurt, R.N.; Kurtulbaş, E.; Şahin, S. Structure-Property Relationships Governing Encapsulation and Release of Antibiotics from Calcium–Alginate Hydrogels. *Gels* **2026**, *12*, 636. [CrossRef]
5. Benfattoum, K.; Haddadine, N.; Bouslah, N.; Benaboura, A.; Maincent, P.; Barillé, R.; Sapin-Minet, A.; El-Shall, M.S. Formulation Characterization and in Vitro Evaluation of Acacia Gum–Calcium Alginate Beads for Oral Drug Delivery Systems. *Polym. Adv. Technol.* **2018**, *29*, 884–895. [CrossRef]
6. Gaur, P.K.; Mishra, S.; Kumar, A.; Panda, B.P. Development and Optimization of Gastroretentive Mucoadhesive Microspheres of Gabapentin by Box-Behnken Design. *Artif. Cells Nanomed. Biotechnol.* **2014**, *42*, 167–177. [CrossRef]
7. Essifi, K.; Lakrat, M.; Berraaouan, D.; Fauconnier, M.L.; El Bachiri, A.; Tahani, A. Optimization of Gallic Acid Encapsulation in Calcium Alginate Microbeads Using Box-Behnken Experimental Design. *Polym. Bull.* **2020**, *78*, 5789–5814. [CrossRef]
8. Kurtulbaş, E.; Albarri, R.; Torun, M.; Şahin, S. Encapsulation of Moringa Oleifera Leaf Extract in Chitosan-Coated Alginate Microbeads Produced by Ionic Gelation. *Food Biosci.* **2022**, *50*, 102158. [CrossRef]
9. Krunic, T.; Ilic, N.; Osmokrovic, A. Effect of Biopolymer Additives on Functional Properties of Alginate-Based Composite Hydrogels. *Gels* **2026**, *12*, 266. [CrossRef]
10. Sıçramaz, H. Structure–Mechanical Relationships in Alginate–Chitosan Polymer Composites. *Polymers* **2026**, *18*, 713. [CrossRef]
11. Wawrzyńczak, A.; Kłosowska, A.; Feliczak-Guzik, A. Polysaccharide-Based Organic-Inorganic Hybrid Carriers with Alginate as a Reference Matrix: Structure-Property Relationships and Emerging Applications in Encapsulation and Controlled Release. *Polymers* **2026**, *18*, 2047. [CrossRef]
12. Omer, A.M.; Ahmed, M.S.; El-subruiti, G.M.; Khalifa, R.E.; Eltaweil, A.S. PH-Sensitive Alginate/Carboxymethyl Chitosan/Aminated Chitosan Microcapsules for Efficient Encapsulation and Delivery of Diclofenac Sodium. *Pharmaceutics* **2021**, *13*, 338. [CrossRef]
13. Cristino, J.H.S.; Guedes, J.M.; Sachse, A.; Santos, A.G.D.; da Silva Caldeira, V.P.; dos Santos, H.S. Hydrogel-Based Strategies for the Controlled Delivery of Analgesic and Anti-Inflammatory Drugs. *Chem. Pap.* **2026**, 1–17. [CrossRef]
14. Miastkowska, A.; Sikora, M.; Vodnar, C.; Etocha, A.; Miastkowska, M.; Zbieta Sikora, E. Preparation and Characteristics of Alginate Microparticles for Food, Pharmaceutical and Cosmetic Applications. *Polymers* **2022**, *14*, 3834. [CrossRef]
15. Celli, G.B.; Ghanem, A.; Brooks, M.S.L. Optimized Encapsulation of Anthocyanin-Rich Extract from Haskap Berries (Lonicera Caerulea L.) in Calcium-Alginate Microparticles. *J. Berry Res.* **2016**, *6*, 1–11. [CrossRef]
16. Takka, S.; Gürel, A. Evaluation of Chitosan/Alginate Beads Using Experimental Design: Formulation and in Vitro Characterization. *AAPS PharmSciTech* **2010**, *11*, 460–466. [CrossRef]
17. Arauzo, B.; González-Garcinuño, Á.; Tabernero, A.; Calzada-Funes, J.; Lobera, M.P.; del Valle, E.M.M.; Santamaria, J. Engineering Alginate-Based Dry Powder Microparticles to a Size Suitable for the Direct Pulmonary Delivery of Antibiotics. *Pharmaceutics* **2022**, *14*, 2763. [CrossRef]
18. George, M.; Abraham, T.E. Polyionic Hydrocolloids for the Intestinal Delivery of Protein Drugs: Alginate and Chitosan—a Review. *J. Control. Release* **2006**, *114*, 1–14. [CrossRef]
19. Essifi, K.; Brahmi, M.; Berraaouan, D.; Ed-Daoui, A.; El Bachiri, A.; Fauconnier, M.L.; Tahani, A. Influence of Sodium Alginate Concentration on Microcapsules Properties Foreseeing the Protection and Controlled Release of Bioactive Substances. *J. Chem.* **2021**, *2021*, 5531479. [CrossRef]
20. Amiruddin, A.; Rahmadi, M.; Melani Hariyadi, D. A Review on Calcium-Alginate Microspheres for Drug Delivery System: Characteristics, Drug Release, Activity, Stability and In Vivo Studies. *J. Pharm. Sci.* **2025**, *50*, 169–186. [CrossRef]
21. Kulkarni, A.R.; Soppimath, K.S.; Aminabhavi, T.M. Controlled Release of Diclofenac Sodium from Sodium Alginate Beads Crosslinked with Glutaraldehyde. *Pharm. Acta Helv.* **1999**, *74*, 29–36. [CrossRef]
22. Nayak, A.K.; Khatua, S.; Hasnain, M.S.; Sen, K.K. Development of Diclofenac Sodium-Loaded Alginate-PVP K 30 Microbeads Using Central Composite Design. *Daru* **2011**, *19*, 356.
23. Siaw Paw, J.K.; Kiong, T.S.; Kamarulzaman, M.K.; Adam, A.; Hisham, S.; Kadirgama, K.; Ramasamy, D.; Yaw, C.T.; Yusop, A.F.; Yusaf, T.; et al. Advancing Renewable Fuel Integration: A Comprehensive Response Surface Methodology Approach for Internal Combustion Engine Performance and Emissions Optimization. *Heliyon* **2023**, *9*, e22238. [CrossRef]
24. Bisht, D.; Yadav, S.K.; Darmwal, N.S. Computation of Interactive Effects and Optimization of Process Parameters for Alkaline Lipase Production by Mutant Strain of Pseudomonas Aeruginosa Using Response Surface Methodology. *Braz. J. Microbiol.* **2013**, *44*, 245–252. [CrossRef]

25. Mackin-Mohamour, A.R.S.; Budzinski, J.; Bastogne, T.; Roques-Carmes, T.; Sadtler, V.; Marchal, P.; Sapin-Minet, A.; Parent, M. Agile Quality-by-Design Development of Alginate Microparticles for Encapsulation of Hydrophilic Drug. *Colloids Surf. A Physicochem. Eng. Asp.* **2024**, *693*, 134053. [CrossRef]
26. Abul Kalam, M.; Khan, A.A.; Khan, S.; Almalik, A.; Alshamsan, A. Optimizing Indomethacin-Loaded Chitosan Nanoparticle Size, Encapsulation, and Release Using Box–Behnken Experimental Design. *Int. J. Biol. Macromol.* **2016**, *87*, 329–340. [CrossRef]
27. Ramdhan, T.; Ching, S.H.; Prakash, S.; Bhandari, B. Time Dependent Gelling Properties of Cuboid Alginate Gels Made by External Gelation Method: Effects of Alginate-CaCl2 Solution Ratios and PH. *Food Hydrocoll.* **2019**, *90*, 232–240. [CrossRef]
28. Toprakçı, G.; Toprakçı, İ.; Şahin, S. Alginate Microbeads for Trapping Phenolic Antioxidants in Rosemary (Rosmarinus Officinalis L.): Multivariate Optimization Based on Bioactive Properties and Morphological Measurements. *Gels* **2025**, *11*, 172. [CrossRef]
29. Dodero, A.; Pianella, L.; Vicini, S.; Alloisio, M.; Ottonelli, M.; Castellano, M. Alginate-Based Hydrogels Prepared via Ionic Gelation: An Experimental Design Approach to Predict the Crosslinking Degree. *Eur. Polym. J.* **2019**, *118*, 586–594. [CrossRef]
30. Alkhatib, H.; Doolaanea, A.A.; Assadpour, E.; Mohmad Sabere, A.S.; Mohamed, F.; Jafari, S.M. Optimizing the Encapsulation of Black Seed Oil into Alginate Beads by Ionic Gelation. *J. Food Eng.* **2022**, *328*, 111065. [CrossRef]
31. Boukhatem, G.; Bencheikh, M.; Bekkouche, S.R.; Kırgız, M.S.; Manikandan, D.; Krishnaraj, R. Data-Driven Optimization and Pressuremeter Modulus Prediction Using Response Surface Methodology for Smarter Geotechnical Design. *Sci. Rep.* **2026**, *16*, 5679. [CrossRef]
32. Martín-López, R.; Puente-Santamaría, A.; Rubio, R.G.; Ortega, F.; Guzmán, E. Formation and Interfacial Behavior of Chitosan–Alginate Interpolyelectrolyte Complexes: From Bulk Dispersions to Layer-by-Layer Films. *Polymers* **2025**, *17*, 3073. [CrossRef]
33. Çetin, M. Combination of Alginate and Chitosan Polymers in the Preparation of Nanoparticles-A Mini Review. *Int. J. PharmATA* **2023**, *1*, 19–26.
34. Pan, J.; Li, Y.; Chen, K.; Zhang, Y.; Zhang, H. Enhanced Physical and Antimicrobial Properties of Alginate/Chitosan Composite Aerogels Based on Electrostatic Interactions and Noncovalent Crosslinking. *Carbohydr. Polym.* **2021**, *266*, 118102. [CrossRef]
35. Meskelis, L.; F. Agondi, R.; Duarte, L.G.R.; de Carvalho, M.D.; Sato, A.C.K.; Picone, C.S.F. New Approaches for Modulation of Alginate-Chitosan Delivery Properties. *Food Res. Int.* **2024**, *175*, 1137317. [CrossRef]
36. Hou, D.; Gui, R.; Hu, S.; Huang, Y.; Feng, Z.; Ping, Q. Preparation and Characterization of Novel Drug-Inserted-Montmorillonite Chitosan Carriers for Ocular Drug Delivery. *Adv. Nanopart.* **2015**, *4*, 70–84. [CrossRef]
37. Javed, S.; Abbas, G.; Shah, S.; Rasul, A.; Irfan, M.; Saleem, A.; Hosny, K.M.; Bukhary, S.M.; Safhi, A.Y.; Sabei, F.Y.; et al. Tobramycin-Loaded Nanoparticles of Thiolated Chitosan for Ocular Drug Delivery: Preparation, Mucoadhesion and Pharmacokinetic Evaluation. *Heliyon* **2023**, *9*, e19877. [CrossRef]
38. Piegat, A.; Żywicka, A.; Niemczyk, A.; Goszczyńska, A. Antibacterial Activity of N,O-Acylated Chitosan Derivative. *Polymers* **2021**, *13*, 107. [CrossRef]
39. Chica, L.R.; Yamashita, C.; Nunes, N.S.S.; Negreiros, A.T.; Moraes, I.C.F.; Ferreira, A.G.; Mayer, C.R.M.; Haminiuk, C.W.I.; Branco, C.C.Z.; Branco, I.G. Optimizing Alginate Extraction Using Box-Behnken Design: Improving Yield and Antioxidant Properties through Ultrasound-Assisted Citric Acid Extraction. *Food Chem. Adv.* **2024**, *5*, 100813. [CrossRef]
40. Jiménez-Contreras, L.F.; Ariza-Castolo, A.; Díaz-Fernández, M.; Sarmiento-Gómez, E.; Barrón-Zambrano, J.A.; Fernández-Herrera, M.A. Extraction Route Controls the Microstructure and Rheological Performance of Sodium Alginate from Beach-Cast Sargassum Spp. *Polysaccharides* **2026**, *7*, 74. [CrossRef]
41. Lekgoathi, M.D.S.; Le Roux, J.P. Attenuated Total Reflectance Powder Cell for Infrared Analysis of Hygroscopic Samples. *Spectrochim. Acta A Mol. Biomol. Spectrosc.* **2011**, *82*, 529–531. [CrossRef]
42. Zauska, L.; Bova, S.; Benova, E.; Bednarcik, J.; Balaz, M.; Zelenak, V.; Hornebecq, V.; Almasi, M. Thermosensitive Drug Delivery System SBA-15-PEI for Controlled Release of Nonsteroidal Anti-Inflammatory Drug Diclofenac Sodium Salt: A Comparative Study. *Materials* **2021**, *14*, 1880. [CrossRef]
43. Choi, I.; Lee, Y.; Lyu, J.S.; Lee, J.S.; Han, J. Characterization of Ionically Crosslinked Alginate Films: Effect of Different Anion-Based Metal Cations on the Improvement of Water-Resistant Properties. *Food Hydrocoll.* **2022**, *131*, 107785. [CrossRef]
44. Ghoneum, M.; Kenawy, E.R.; Soliman, H.M.A.; Abdel-Moaty, M.S.; El-Shanshory, A.A. Chitosan || Biobran/PVA || Chitosan/PVA Tri-Layered Nanofiber Scaffold: A Biphasic Release System with Physicochemical Properties Conducive to Skin Tissue Engineering. *Carbohydr. Polym. Technol. Appl.* **2025**, *11*, 100878. [CrossRef]
45. Tomaz, A.F.; de Carvalho, S.M.S.; Barbosa, R.C.; Silva, S.M.L.; Gutierrez, M.A.S.; de Lima, A.G.B.; Fook, M.V.L. Ionically Crosslinked Chitosan Membranes Used as Drug Carriers for Cancer Therapy Application. *Materials* **2018**, *11*, 2051. [CrossRef]
46. Wibowo, S.; Velazquez, G.; Savant, V.; Torres, J.A. Surimi Wash Water Treatment for Protein Recovery: Effect of Chitosan-Alginate Complex Concentration and Treatment Time on Protein Adsorption. *Bioresour. Technol.* **2005**, *96*, 665–671. [CrossRef]
47. Abubakr, N.; Lin, S.X.; Chen, X.D. Effects of Drying Methods on the Release Kinetics of Vitamin B12 in Calcium Alginate Beads. *Dry. Technol.* **2009**, *27*, 1258–1265. [CrossRef]

48. Martinović, J.; Lukinac, J.; Jukić, M.; Ambrus, R.; Planinić, M.; Šelo, G.; Perković, G.; Bucić-Kojić, A. The Release of Grape Pomace Phenolics from Alginate-Based Microbeads during Simulated Digestion In Vitro: The Influence of Coatings and Drying Method. *Gels* **2023**, *9*, 870. [CrossRef]
49. Manjili, Z.N.; Mahoonak, A.S.; Ghorbani, M.; Tabarestani, H.S. Multi-Layer Encapsulation of Pumpkin (*Cucurbita Maxima* L.) Seed Protein Hydrolysate and Investigating Its Release and Antioxidant Activity in Simulated Gastrointestinal Digestion. *Heliyon* **2024**, *10*, e29669. [CrossRef]
50. Park, K.H.; Choi, Y.W.; Ryu, H.; Lee, H.J.; Moon, J.-H.; Song, H.-J.; Park, Y.-J. Controlled Drug Release Using Chitosan-Alginate-Gentamicin Multi-Component Beads. *Materials* **2022**, *15*, 7682. [CrossRef]
51. Caetano, L.A.; Almeida, A.J.; Gonçalves, L.M.D. Effect of Experimental Parameters on Alginate/Chitosan Microparticles for BCG Encapsulation. *Mar. Drugs* **2016**, *14*, 90. [CrossRef]
52. Ibrahim, H.K.; Sorour, R.M.H.; Salah Ad-din, I. Application of Mathematical Modelling to Alginate Chitosan Polyelectrolyte Complexes for the Prediction of System Behavior with Venlafaxine HCl as a Model Charged Drug. *Saudi Pharm. J.* **2022**, *30*, 1507–1520. [CrossRef]
53. Jeong, H.-S.; Kim, H.-J.; Kang, S.-M.; Choi, C.-H. Surfactant-Free Electrosprayed Alginate Beads for Oral Delivery of Hydrophobic Compounds. *Polymers* **2025**, *17*, 2098. [CrossRef]
54. Bhattacharjee, S. DLS and Zeta Potential—What They Are and What They Are Not? *J. Control. Release* **2016**, *235*, 337–351. [CrossRef]
55. Dash, S.; Murthy, P.N.; Nath, L.; Chowdhury, P. Kinetic Modeling on Drug Release from Controlled Drug Delivery Systems. *Acta Pol. Pharm.-Drug Res.* **2010**, *67*, 217–223.
56. González-Rodríguez, M.L.; Holgado, M.A.; Sánchez-Lafuente, C.; Rabasco, A.M.; Fini, A. Alginate/Chitosan Particulate Systems for Sodium Diclofenac Release. *Int. J. Pharm.* **2002**, *232*, 225–234. [CrossRef]
57. Unagolla, J.M.; Jayasuriya, A.C. Drug Transport Mechanisms and in Vitro Release Kinetics of Vancomycin Encapsulated Chitosan-Alginate Polyelectrolyte Microparticles as a Controlled Drug Delivery System. *Eur. J. Pharm. Sci.* **2018**, *114*, 199–209. [CrossRef]
58. Jin, X.; Wang, Q.; Sun, J.; Panezai, H.; Bai, S.; Wu, X. Dual (PH- and Temperature-) Stimuli Responsive Nanocarrier with Bimodal Mesoporous Silica Nanoparticles Core and Copolymer Shell for Controlled Ibuprofen-Releasing: Fractal Feature and Diffusion Mechanism. *Microporous Mesoporous Mater.* **2017**, *254*, 77–85. [CrossRef]
59. Navarro-Flores, M.J.; Ventura-Canseco, L.M.C.; Meza-Gordillo, R.; Ayora-Talavera, T.d.R.; Abud-Archila, M. Spray Drying Encapsulation of a Native Plant Extract Rich in Phenolic Compounds with Combinations of Maltodextrin and Non-Conventional Wall Materials. *J. Food Sci. Technol.* **2020**, *57*, 4111–4122. [CrossRef]
60. Lakshani, N.; Wijerathne, H.S.; Sandaruwan, C.; Kottegoda, N.; Karunarathne, V. Release Kinetic Models and Release Mechanisms of Controlled-Release and Slow-Release Fertilizers. *ACS Agric. Sci. Technol.* **2023**, *3*, 939–956. [CrossRef]
61. Zeiringer, S.; Wiltschko, L.; Brandl, B.; Palanisamy, A.; Nguyen, T.; Katschnig, M.; Spoerk, M.; Eder, S.; Roblegg, E. Dynamic versus Static In Vitro Drug Release Testing of Subcutaneous Implants with Distinct Microstructures. *ACS Omega* **2026**, *11*, 41989–42000. [CrossRef]
62. Safitri, A.; Sutrisno, S.; Wardhani, S.; Azhar, H.Z.; Affan, A.; Fadhilah, R.F. Spray-Drying Microencapsulation of Nigella Sativa Extract: Antioxidant Activity and PH-Responsive Intestinal Release. *CYTA-J. Food* **2025**, *23*, 2609413. [CrossRef]

Disclaimer/Publisher's Note: The statements, opinions and data contained in all publications are solely those of the individual author(s) and contributor(s) and not of MDPI and/or the editor(s). MDPI and/or the editor(s) disclaim responsibility for any injury to people or property resulting from any ideas, methods, instructions or products referred to in the content.